Dovepress
Taylor & Francis Group

ORIGINAL RESEARCH

Based on Soluble Immune Checkpoints Constructing a Random Survival Forest Model to Predict the Prognosis of Hepatitis B Virus-Associated Hepatocellular Carcinoma

Xue Cai [1,2,*], Lihua Yu [1,*], Xiaoli Liu[1], Huiwen Yan [1], Yuqing Xie[1], Qing Pu[3], Zimeng Shang[1], Yuan Wu [4], Tingting Jiang [1], Zhiyun Yang [1]

[1]Center of Integrative Medicine, Beijing Ditan Hospital, Capital Medical University, Beijing, 100015, People's Republic of China; [2]Beijing Shangdi Hospital, Beijing, 100085, People's Republic of China; [3]School of Traditional Chinese Medicine, Capital Medical University, Beijing, 100069, People's Republic of China; [4]School of Basic Medical Sciences, Chengdu University of Traditional Chinese Medicine, Chengdu, 611137, People's Republic of China

*These authors contributed equally to this work

Correspondence: Zhiyun Yang, Center for Integrative Medicine, Beijing Ditan Hospital, Capital Medical University, Bei-Jing, 100015, People's Republic of China, Email Yangzhiyun2016@163.com

Background: Nowadays, immune checkpoint blockade (ICB) therapy has become a milestone in immunotherapy for hepatocellular carcinoma (HCC). However, its clinical effectiveness remains low. Soluble (s) immune checkpoints (ICs), functional components of membrane ICs, are novel physiological immunomodulators. We investigated the prognostic value of sICs in patients of hepatitis B virus-associated hepatocellular carcinoma (HBV-HCC) and provided clinical clues for potential new targets for future immunotherapy.

Methods: A total of 256 participants were included in this study. We compared the plasma levels of 14 sICs in healthy controls (HC), chronic hepatitis B (CHB), hepatitis B-related liver cirrhosis (HBV-LC), and HBV-HCC groups. COX and random survival forest (RSF) were used to select variables and construct a model to predict overall survival of patients with HBV-HCC. We evaluated the predictive efficacy and analyzed the correlations between sICs, clinical parameters, and membrane ICs.

Results: The levels of 14 sICs in HBV-HCC were elevated compared to that in HC. The areas under the receiver operating characteristic values of 1-, 2-, and 3-year survival predicted by the RSF model were 0.96, 0.85, and 0.81 in the training set, and 0.91, 0.80, and 0.71 in the validation set. The model could adapt to different event distributions and clinical staging systems. Soluble glucocorticoid—induced tumor necrosis factor receptor (sGITR), soluble programmed cell death-ligand 1 (sPD-L1) and soluble T cell immunoglobulin and mucin domain-containing protein 3 (sTIM-3) were closely associated with the prognosis of patients. Soluble PD-L1 was negatively correlated with HGB and positively correlated with AST and NLR ($P < 0.05$). Soluble TIM-3 was negatively correlated with ALB and CD8+ T cells and positively correlated with HBV-DNA, AST, LDH and mTIM-3 expression in CD8+ T cells ($P<0.05$).

Conclusion: We constructed a predictive model based on sICs to predict different survival times in HBV-HCC patients. The risk stratification effectively identified potentially critical patients. Soluble GITR, sPD-L1 and sTIM-3 were important immunological indicators which could dynamically monitor patients' immune status.

Keywords: hepatitis B virus-associated hepatocellular carcinoma, soluble immune checkpoints, prognosis, random survival forest model, overall survival

Introduction

Liver cancer is one of the most common and third leading causes of cancer-related deaths worldwide.[1] Hepatocellular carcinoma (HCC) is the most common form of liver cancer, accounting for approximately 90% of cases.[2] Hepatitis B virus (HBV) infection is one of the most important etiological factors for HCC in Asia.[3] Most patients are diagnosed at an advanced stage of disease. This limits treatment options and leads to high mortality rates. Currently, revolutionary advances in immune checkpoint blockade

Graphical Abstract
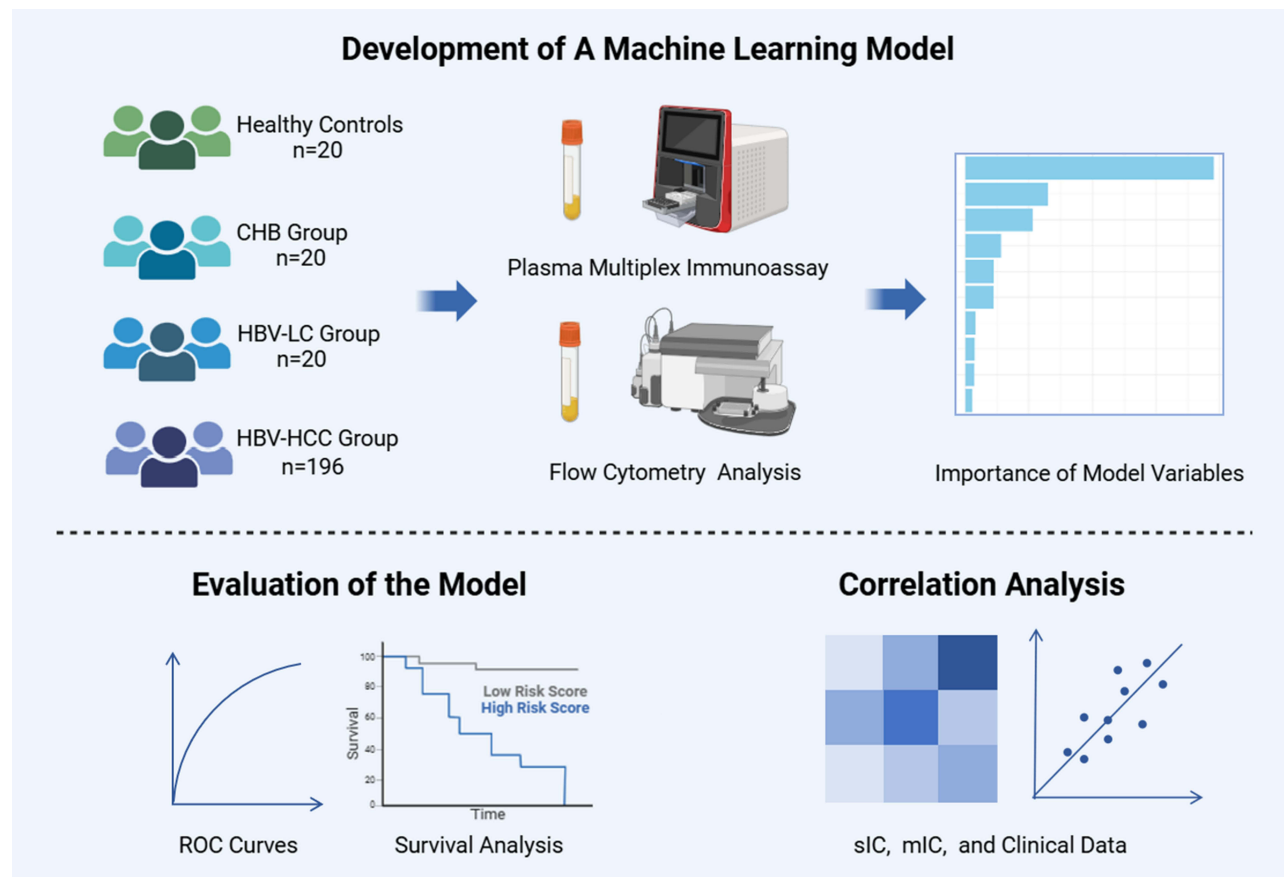
(ICB) therapies, such as anti-PD-1/L1 and anti-CTLA4 antibodies, have prolonged the survival of patients with HCC. However, the response of patients with HCC to ICB remains limited.[4] Therefore, gaining insight into the mechanisms of the hepatitis B virus-related hepatocellular carcinoma (HBV-HCC) tumor microenvironment and identifying biomarkers for accurately predicting the immunotherapeutic response and prognosis of HBV-HCC represent an area of clinical significance.

In recent years, researchers have identified a series of soluble immune checkpoints (sICs) that may contribute to intrahepatic CD8+ T cell dysfunction and correlate with prognosis in patients with HBV-HCC.[5–8] These molecules, such as sPD-L1, can bind to immune checkpoint inhibitors, thereby affecting the efficacy of ICB.[9] sPD-L1 also binds to PD-1 on T cells, dampening anti-tumor immunity.[10] sGITR activates inflammatory pathways in murine models and induces cell cycle progression inhibition along with programmed cell death in mouse-derived macrophages.[11,12] sTIM-3 decreases anti-tumor CD8+ T cell activity and reduces the abundance of infiltrative lymphocytes in tumors.[13] They are mainly produced via mRNA translation or the shedding of membrane-binding immune checkpoints, and bind to receptors or ligands on the cell membrane.[14] Several clinical studies have evaluated their prognostic value in patients with cancer.[15,16] However, few studies have been conducted on sICs in blood, especially in patients with HBV-HCC.

In this study, we firstly systematically evaluated the prognostic value of various sICs for the survival of HBV-HCC patients, identifying sGITR, sPD-L1, and sTIM-3 as novel negative prognostic risk factors. This finding highlighted the unique immune landscape of HBV-HCC, where chronic viral infection and tumor-driven immune evasion synergistically shape the soluble checkpoint profile. Importantly, sGITR have not been previously linked to HBV-HCC prognosis. Additionally, there were relatively few prognostic models for HCC that incorporate both immune and clinical indicators. Random Survival Forest (RSF) algorithm precisely captured complex synergistic interactions among diverse risk factors,

and successfully constructed temporally interpretable individualized survival curves. We innovatively constructed an RSF model based on sICs and clinical parameters to predict the 3-year overall survival (OS) of HBV-HCC patients. Unlike prior studies focusing solely on sPD-L1 in HCC, our multi-sIC analysis revealed a combinatorial prognostic signature (sGITR+sPD-L1+sTIM-3) with higher predictive accuracy.

Materials and Methods

Study Design and Participants

The Ethics Committee of Beijing Ditan Hospital of the Capital Medical University authorized this study. We obtained the written informed consent and collected corresponding blood samples and clinical data from all the participants at enrollment. A schematic of the design of this study was shown in Figure 1. First, we examined the concentration of sICs in the plasma of healthy controls (HC), the chronic hepatitis B (CHB) group, the hepatitis B-related liver cirrhosis (HBV-LC) group, and the HBV-HCC group. Then, in accordance with the principle of randomization, the patients were divided into a training set (n=138) and a validation set (n=58) in a ratio of 7:3. We constructed an RSF model and evaluated its predictive and prognostic value. Finally, we analyzed the correlation between sICs, clinical parameters, and membrane ICs.

We recruited patients with HBV-HCC who were hospitalized between May 2017 and June 2020 at Beijing Ditan Hospital. The inclusion criteria were as follows: (i) complying with the clinical diagnosis of HCC, (ii) complying with the diagnosis of chronic HBV infection, and (iii) age between 18 and 75 years old. The exclusion criteria were as follows: (i) cholangiocarcinoma, (ii) metastatic HCC, (iii) other types of cancer, (iv) lost to follow-up, (v) severe diseases of important organs, and (vi) incomplete clinical data. We assessed the survival status and disease progression of patients every 3 months by electronic medical records and telephone follow-up visits. The time from enrollment to death was defined as overall survival time.

Sample and Data Collection

We collected baseline plasma samples from patients with confirmed HBV-HCC. Simultaneously, we collected plasma from healthy people, CHB patients, and HBV-LC patients matched for age and sex as controls. Venipuncture was
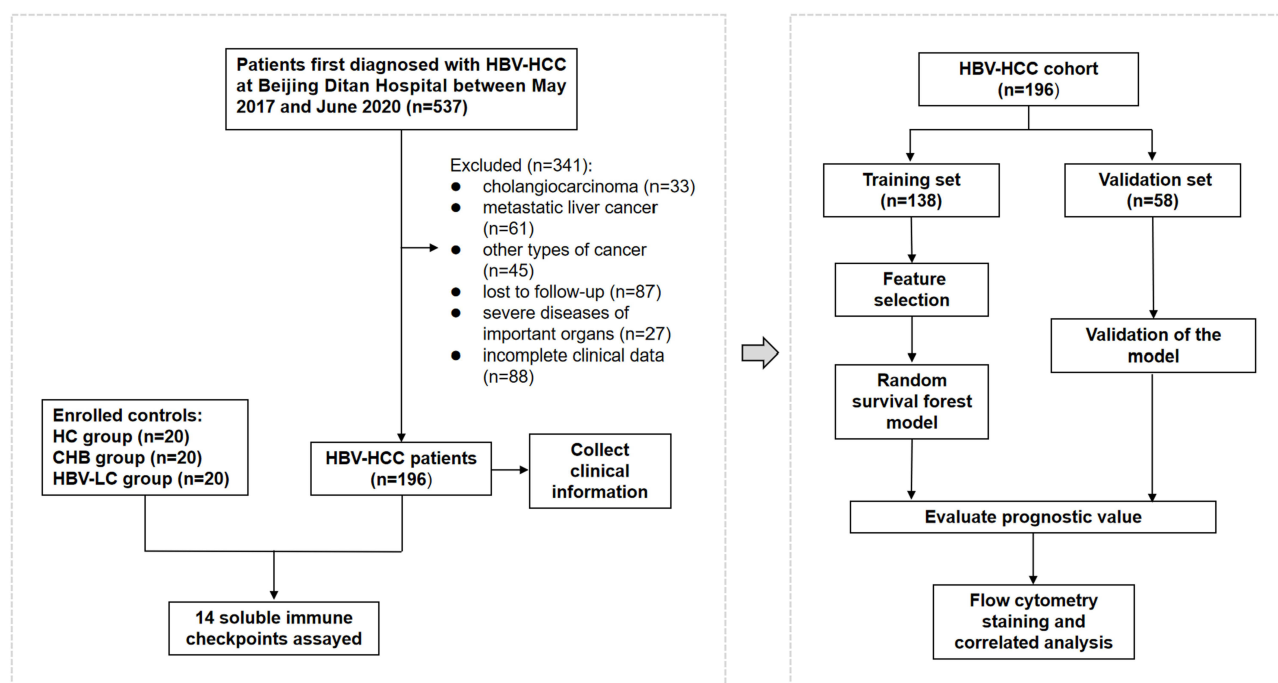
Figure 1 A flow chart describing the process of research and data analysis.

performed to obtain peripheral blood samples from the enrolled patients. We centrifuged to isolate the plasma. Plasma samples were frozen at −80 °C pending analysis. At the same time, we collected the baseline clinical data of the patients and control groups. Data missing at a moderate rate (<5.1%) were replaced via multiple imputation. To compare the levels of sICs across the four groups, during data preprocessing, all feature values were log2 transformed to reduce outliers and approximate a Gaussian distribution for numerical features (Figure 2).

Plasma Multiplex Immunoassay

The Immuno-Oncology Checkpoint 14-Plex Human ProcartaPlex Panel 1 (EPX14A-15803-901) was used to analyze plasma samples. All tests were performed using a Luminex 200 instrument, according to the manufacturer's instructions, as previously reported. The ProcartaPlex Analyst software (version 1.0) was used for data analysis. The concentration of sICs (pg/mL) was calculated by fitting a standard curve of the average fluorescence intensity versus concentration.

Flow Cytometry Staining and Analysis

The Ficoll-Paque (Amersham Pharmacia Biotech) density gradient centrifugation was used to isolate the peripheral blood mononuclear cells (PBMC). PBMCs and conjugated antibodies were incubated at 4°C for 30 min in the dark, washed, and further subjected to flow cytometry. 7-AAD viability dye (BD Biosciences, #51-68981E) staining solution was added to samples before analysis to remove dead cells. T cell surface molecules were analyzed by flow cytometry using the following reagents: anti-human CD3-BV786 (clone SK7; 563800), anti-human CD4-APC-Fire750 (clone SK3; 980814), anti-human CD8-BV510 (clone SK1; 344732), anti-human TIM-3-FITC (clone F38-2E2; 11–3109-42). NK cell surface molecules were analyzed by flow cytometry using the following reagents: anti-human CD3-BV786 (clone SK7; 563800),
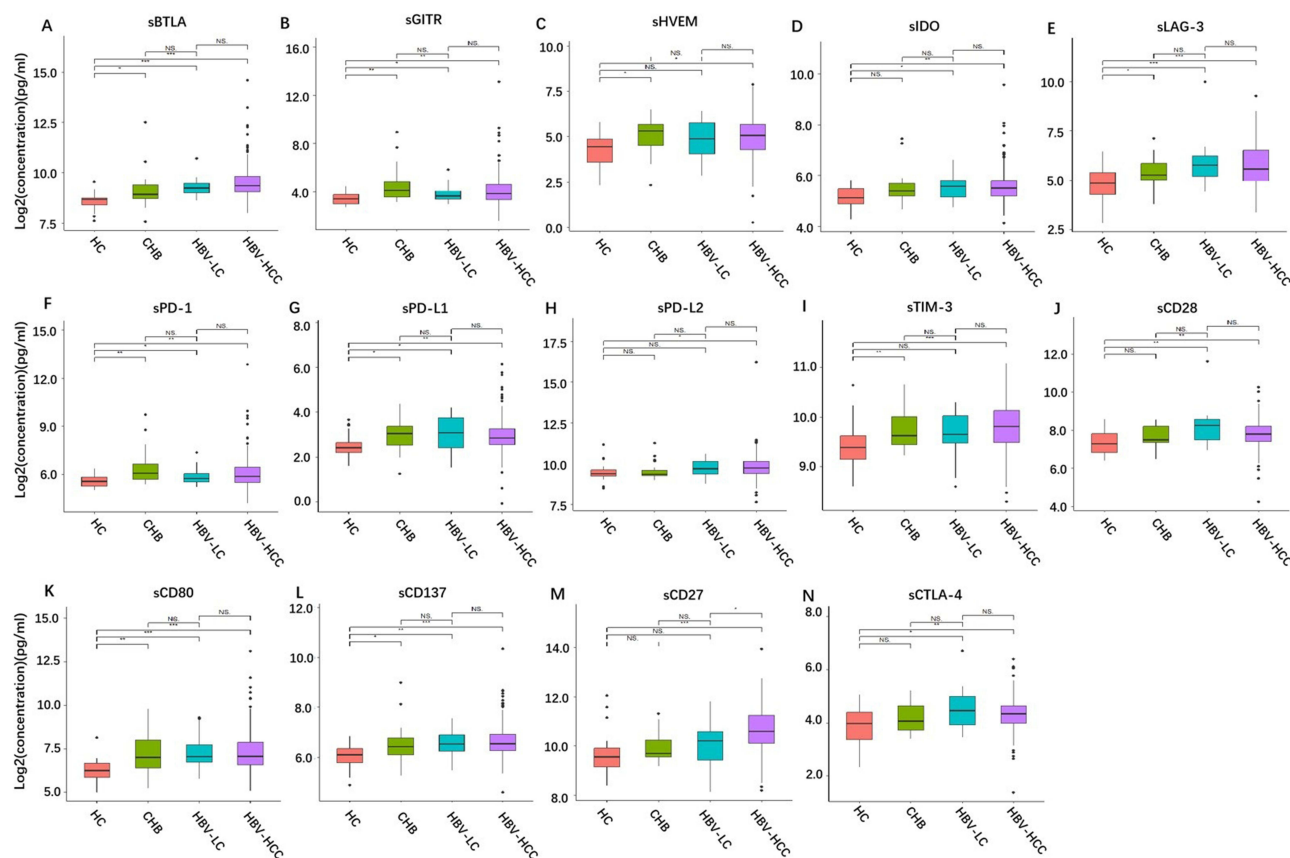
Figure 2 Comparison of 14 sICs levels among HC (n=20), CHB (n=20), HBV-LC (n=20) and HBV-HCC (n=196) groups. Differences in Log2sBTLA (**A**), Log2sGITR (**B**), Log2sHVEM (**C**), Log2sIDO (**D**), Log2sLAG-3 (**E**), Log2sPD-1 (**F**), Log2sPD-L1 (**G**), Log2sPD-L2 (**H**), Log2sTIM-3 (**I**), Log2sCD28 (**J**), Log2sCD80 (**K**), Log2sCD137 (**L**), Log2sCD27 (**M**) and Log2sCTLA-4 (**N**) concentration among the four groups. Comparisons between two groups were made using the Mann–Whitney U-test. *p < 0.05; **p < 0.01; ***p < 0.001; NS, no significance.

anti-human CD14-BV650 (clone M5E2; 563419), anti-human CD19-APC-H7 (clone SJ25C1; 560,177), anti-human CD56-BV510 (clone HCD56; 318340), anti-human CD16-BV711 (clone 3G8; 563127), anti-human TIM-3-FITC (clone F38-2E2; 11–3109-42).

Statistical Analysis

T-test or Wilcoxon test were used to compare continuous variables. Chi-square test or Fisher's exact test was used to compare categorical variables. COX regression analysis was used to screen for prognostic factors of patients with HBV-HCC. RSF was used to rank the importance of variables and build a predictive model. RSF was based on the Random Forest algorithm and constructed multiple-decision trees through bootstrap sampling and feature randomness. It optimized the construction of decision trees by using splitting rules based on survival time, thereby enhancing the stability and accuracy of the model. RSF provided a measure of variable importance (VIMP) to assess the impact of each feature on survival outcomes. In the RSF analysis, 5,000 trees were built using the R package Random Forest SRC (version 3.2.2), and the forest terminal node size was 15 and number for the variables tried at each split was 4. The iteration diagram of spanning tree was shown in Figure 3A. Area under the receiver operating characteristic (AUROC) curve, Brier score, and calibration curve were applied to assess the predictive efficiency of the RSF model. We calculated the risk scores for the RSF model and used the surv_cutpoint function of the R language software to find the optimal cut-off points, which ultimately categorized the HBV-HCC patients into a high-risk group and a low-risk group. We used Kaplan–Meier analysis, Log rank tests and COX analysis to compare OS between the different risk groups. Spearman correlation analysis was used to calculate the correlations among the factors. The analysis was conducted using IBM SPSS Statistics 26.0 and R 4.3.1. *P* < 0.05 had statistical significance.

Results

Participant Characteristics

The levels of sICs and clinical characteristics for the four groups were shown in Tables S1 and S2. In terms of age, gender and liver function, there were no statistically significant differences among the four groups of participants. The horizontal differences between each molecule in the four groups are shown in Figure 2. The levels of 14 sICs in HBV-HCC were elevated compared with HC (*P*<0.05). The levels of sCD27 in HBV-HCC were higher than in HBV-LC (*P*<0.05). The levels of sBTLA, sHVEM, sLAG-3, sPD-1, sPD-L1, sTIM-3, sCD80 and sCD137 were elevated in CHB compared with HC (*P*<0.05). The levels of sBTLA, sGITR, sIDO, sLAG-3, sPD-1, sPD-L1, sCD28, sCD80, CD137 and sCTLA-4 were elevated in HBV-LC compared with HC (*P*<0.05). There were no significant concentration differences between patients in the CHB and HBV-LC groups.

To construct a prognostic model based on sICs, we randomly divided 196 patients with HBV-HCC into training and validation sets. The clinical and immunological characteristics of the patients were summarized in Table 1. The cut-off values of laboratory data were clinically normal values. Baseline sICt levels were grouped using median (Table S3). There was no statistically significant difference between the two groups in terms of liver function, BCLC staging, and
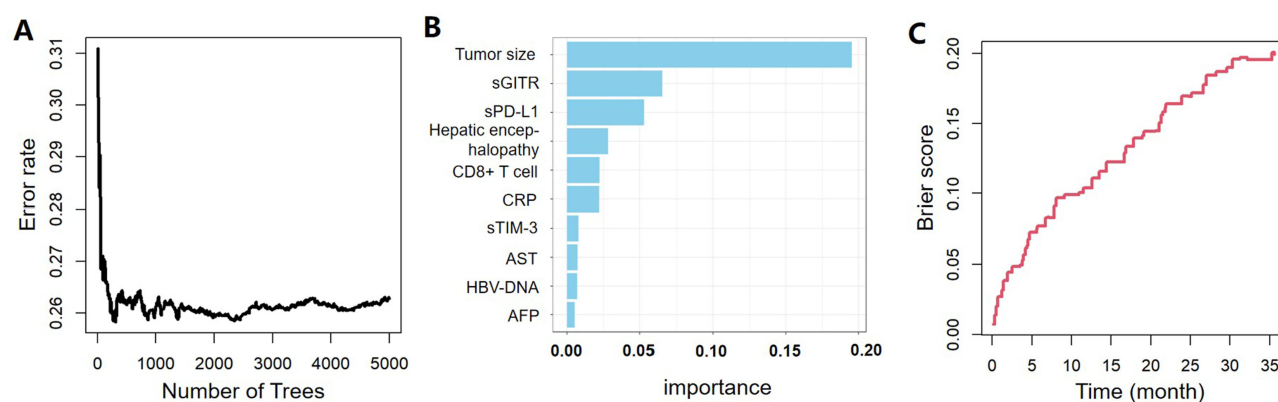
Figure 3 Construction of the random survival forest model. (**A**) Iteration diagram of spanning tree. (**B**) Importance degree of variables. (**C**) Brier score of the model.

Table 1 Baseline Characteristics in Patients with HBV-HCC

Characters		Total Cohort (n=196) %	Training Set (n=138) %	Validation Set (n=58) %	*P* value
Patients background					
Age (year)	<60	93 (47.4)	71 (51.4)	22 (37.9)	0.084
	≥60	103 (52.6)	67 (48.6)	36 (62.1)	
Sex	Male	152 (77.6)	115 (83.3)	37 (63.8)	0.003
	Female	44 (22.4)	23 (16.7)	21 (36.2)	
Alcohol abuse	Yes	73 (37.2)	57 (41.3)	16 (27.6)	0.071
	No	123 (62.8)	81 (58.7)	42 (72.4)	
Hepatic encephalopathy	Yes	12 (6.1)	7 (5.1)	5 (8.6)	0.345
	No	184 (93.9)	131 (94.9)	53 (91.4)	
Gastrointestinal bleeding	Yes	16 (8.2)	10 (7.2)	6 (10.3)	0.471
	No	180 (91.8)	128 (92.8)	52 (89.7)	
Ascites	Yes	88 (44.9)	63 (45.7)	25 (43.1)	0.744
	No	108 (55.1)	75 (54.3)	33 (56.9)	
HBV-DNA (IU/mL)	<500	169 (86.2)	118 (85.5)	51 (87.9)	0.654
	≥500	27 (13.8)	20 (14.5)	7 (12.1)	
Child-Pugh stage	A	89 (45.4)	64 (46.4)	25 (43.1)	0.765
	B	63 (32.1)	43 (31.2)	20 (34.5)	
	C	44 (22.4)	31 (22.4)	13 (22.4)	
BCLC staging	0-B	146 (74.5)	105 (76.1)	41 (70.7)	0.430
	C-D	50 (25.5)	33 (23.9)	17 (29.3)	
Laboratory data					
AST (U/L)	<40	113 (57.7)	83 (60.2)	30 (51.7)	0.277
	≥40	83 (42.3)	55 (39.8)	28 (48.3)	
TBIL (μmol/L)	<18.8	90 (45.9)	63 (45.7)	27 (46.6)	0.908
	≥18.8	106 (54.1)	75 (54.3)	31 (53.4)	
ALB (g/L)	<40	140 (71.4)	97 (70.3)	43 (74.1)	0.587
	≥40	56 (28.6)	41 (29.7)	15 (25.9)	
PTA (%)	<70	58 (29.6)	39 (28.3)	19 (32.8)	0.530
	≥70	138 (70.4)	99 (71.7)	39 (67.2)	
CRP (mg/L)	<5	120 (61.2)	85 (61.6)	35 (60.3)	0.870
	≥5	76 (38.8)	53 (38.4)	23 (39.7)	
CD8+ T cell (cells/μL)	<320	122 (62.2)	87 (63.0)	35 (60.3)	0.723
	≥320	74 (37.7)	51 (36.9)	23 (39.7)	
Tumor-related indicators					
AFP (ng/mL)	<400	156 (79.6)	108 (78.3)	48 (82.8)	0.477
	≥400	40 (20.4)	30 (21.7)	10 (17.2)	
Tumor size (cm)	<5	102 (52)	70 (50.7)	32 (55.2)	0.570
	≥5	94 (48)	68 (49.3)	26 (44.8)	
Tumor number	Solitary	92 (46.9)	67 (48.6)	25 (43.1)	0.487
	Multiple	104 (53.1)	71 (51.4)	33 (56.9)	
Types of treatment	Hepatectomy	6 (3.1)	5 (3.6)	1 (1.7)	0.129
	TACE/RFA	114 (58.1)	84 (60.9)	30 (51.7)	
	Palliative	76 (38.8)	49 (35.5)	27 (46.6)	

Abbreviations: HBV, hepatitis B virus; AST, aspartate aminotransferase; TBIL, total bilirubin; ALB, albumin; PTA, prothrombin time activity; CRP, C-reactive protein; AFP, alpha-fetoprotein; TACE, trans arterial chemoembolization; RFA, radiofrequency ablation.

tumor-related indicators. All patients in this study were Han Chinese. 77.6% of patients were male. In 77.5% of patients, liver function was classified as Child–Pugh A or B. 74.5% of patients were in the early stage of HCC (BCLC stage 0-B). In more than 80% of the patients, the HBV-DNA levels were less than 500 IU/mL.

Feature Selection and RSF Model Construction

We used univariate COX regression analysis for the initial selection of prognostic factors for the 3-year OS in patients with HBV-HCC (Table 2). It indicated that hepatic encephalopathy, ascites, HBV-DNA $\geq$ 500 IU/mL, aspartate aminotransferase (AST) $\geq$ 40U/L, C-reactive protein (CRP) $\geq$ 5 mg/L, CD8+T cell $\geq$ 320 cells/μL, alpha-fetoprotein (AFP) $\geq$ 400 ng/mL, tumor size $\geq$ 5 cm, tumor number $\geq$ 2, sBTLA $\geq$ 665.94 pg/mL, sGITR $\geq$ 75.89 mg/L, sPD-L1 $\geq$ 7.32 mg/L and sTIM-3 $\geq$ 900.24 pg/mL were strongly associated with 3-year OS in patients with HBV-HCC. Next, we constructed an RSF model to predict 3-year OS. In order to include more risk factors related to prognosis, we ranked prognostic variables that exhibited P values less than 0.1 in

**Table 2** Factors Associated with 3-year OS in Patients with HBV-HCC

Variables	Univariate COX Analysis		
	HR	95CI	*P* value
Age (yr), $\geq$ 60	1.118	0.655–1.907	0.628
Sex, male	0.939	0.459–1.922	0.864
Alcohol, yes	1.132	0.662–1.936	0.651
Hepatic encephalopathy, yes	3.089	1.227–7.778	0.017
Gastrointestinal bleeding, yes	1.711	0.682–4.296	0.253
Ascites, yes	1.727	1.011–2.95	0.046
HBV-DNA, $\geq$ 500IU/mL	2.142	1.103–4.157	0.024
AST, $\geq$ 40U/L	2.125	1.245–3.628	0.006
TBIL, $\geq$ 18.8μmol/L	1.031	0.604–1.761	0.91
ALB, $\geq$ 40g/L	0.575	0.303–1.093	0.091
PTA, $\geq$ 70%	0.958	0.528–1.738	0.887
CRP, $\geq$ 5mg/L	2.405	1.407–4.11	0.001
CD8+ T cell, $\geq$ 320cells/μL	0.425	0.228–0.794	0.007
AFP, $\geq$ 400ng/mL	1.955	1.1–3.474	0.022
Tumor size, $\geq$ 5cm	3.437	1.914–6.174	<0.001
Tumor number, $\geq$ 2	1.827	1.051–3.174	0.033
sBTLA, $\geq$ 665.94pg/mL	1.742	1.012–3	0.045
sGITR, $\geq$ 75.89pg/mL	1.84	1.068–3.17	0.028
sHVEM, $\geq$ 31.08pg/mL	0.712	0.416–1.218	0.215
sIDO, $\geq$ 45.87pg/mL	1.139	0.668–1.943	0.632
sLAG-3, $\geq$ 47.76pg/mL	0.772	0.45–1.324	0.347
sPD-1, $\geq$ 59.16pg/mL	0.731	0.425–1.258	0.258
sPD-L1, $\geq$ 7.32pg/mL	2.942	1.655–5.23	<0.001
sPD-L2, $\geq$ 854.08pg/mL	0.91	0.534–1.553	0.73
sTIM-3, $\geq$ 900.24pg/mL	2.296	1.32–3.992	0.003
sCD28, $\geq$ 223.46pg/mL	0.961	0.563–1.638	0.883
sCD80, $\geq$ 134.63pg/mL	1.088	0.637–1.857	0.759
sCD137, $\geq$ 94.03pg/mL	1.149	0.674–1.96	0.61
sCD27, $\geq$ 1543.63pg/mL	1.23	0.721–2.101	0.447
sCTLA-4, $\geq$ 20.36pg/mL	0.915	0.536–1.56	0.743

Abbreviations: HBV, hepatitis B virus; AST, aspartate aminotransferase; TBIL, total bilirubin; ALB, albumin; PTA, prothrombin time activity; CRP, C-reactive protein; AFP, alpha-fetoprotein; sBTLA, soluble B and T Lymphocyte Attenuator; sGITR, soluble Glucocorticoid-Induced TNFR-Related Protein; sHVEM, soluble Herpes Virus Entry Mediator; sIDO, soluble Indoleamine 2.3-Dioxygenase; sLAG-3, soluble Lymphocyte-Activation Gene 3; sPD-1, soluble Programmed Cell Death Protein 1; sPD-L1, soluble Programmed Death-Ligand 1; sPD-L2, soluble Programmed Death-Ligand 2; sTIM-3, soluble T Cell Immunoglobulin and Mucin Domain 3; sCD28, soluble Cluster of Differentiation 28; sCD80, soluble Cluster of Differentiation 80; sCD137, soluble Cluster of Differentiation 137; sCD27, soluble Cluster of Differentiation 27; sCTLA-4, soluble Cytotoxic T-Lymphocyte-Associated Protein 4.

univariate COX regression by RSF. The risk factors *P* values less than 0.1 including hepatic encephalopathy, ascites, HBV-DNA, AST, ALB, CRP, CD8+ T cell, AFP, tumor size, tumor number, sBTLA, sGITR, sPD-L1 and sTIM-3. The predictive model was constructed using a stepwise regression approach. We finally identified the top 10 important prognostic variables and constructed an RSF model, including tumor size, sGITR, sPD-L1, hepatic encephalopathy, CD8+ T cell, CRP, sTIM-3, AST, HBV-DNA and AFP (Figure 3B).

The Evaluation and Interpretation of the RSF Models

Brier score, AUROC, and calibration curves were used to evaluate the performance of the RSF model. The Brier score measured the degree of deviation between predicted and actual outcomes. It calculated the mean squared error between the expected probability and the predicted probability, comprehensively reflecting the discriminative ability and calibration of the model. The range was from 0 to 1, with higher scores indicating worse predicted outcomes and poorer calibration. As shown in Figure 3C, over time, the Brier score of the random survival forest prediction model was less than 0.2, indicating that the model's predictive accuracy was relatively good. Then, we used the AUROC curve to assess the discriminative ability of the model. The AUROC values of 1-, 2-, and 3-year survival predicted by the RSF model were 0.96, 0.85, and 0.81 in the training set, and 0.91, 0.80, and 0.71 in the validation set (Figure 4A and B). Taking into account the continuity of survival time, we used time-dependent AUROC analysis in both the training and validation sets,
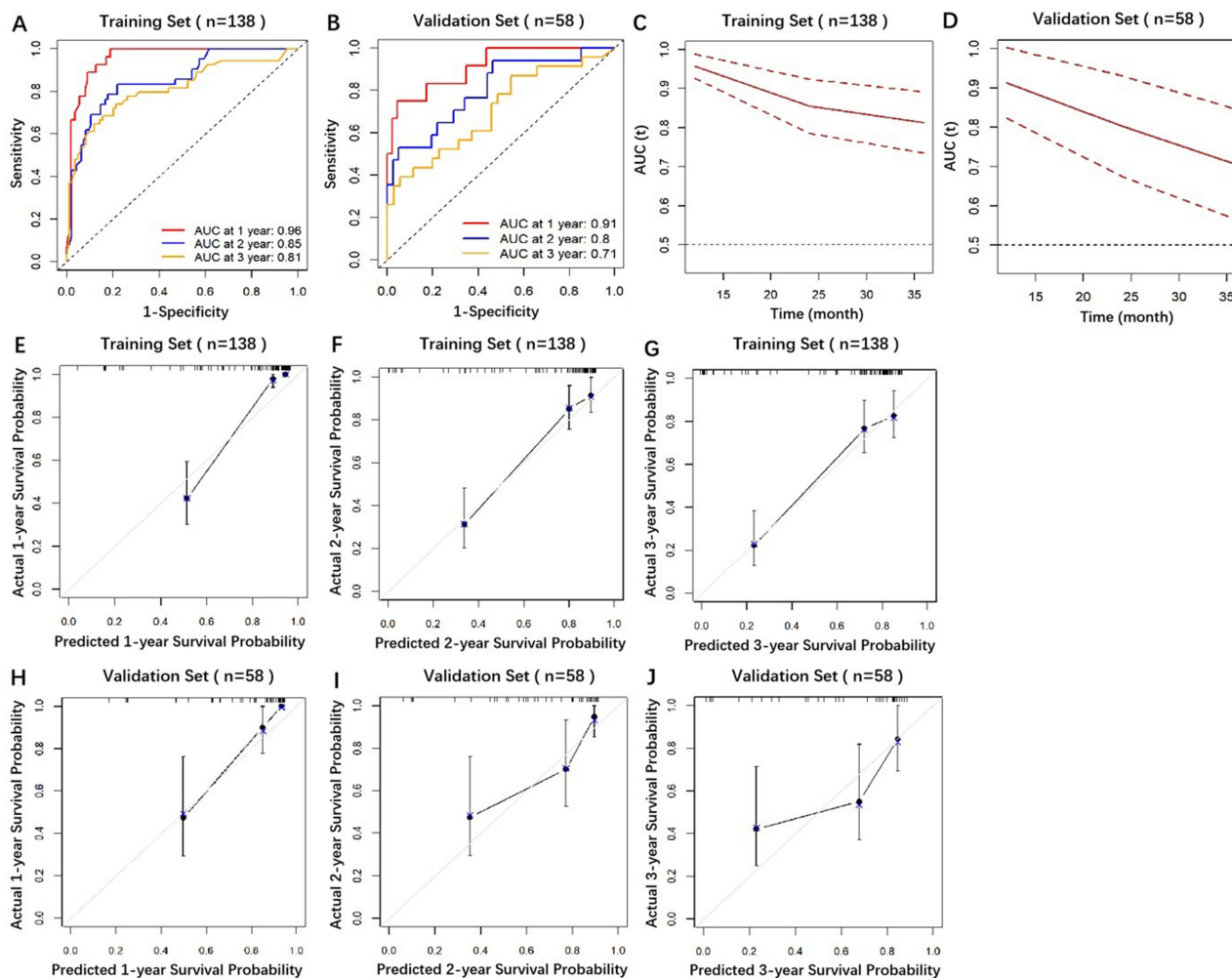

Figure 4 Performance of RSF model to predict OS of patients with HBV-HCC. (**A** and **B**) ROC curves of 1-, 2- and 3-year OS for evaluating the discrimination ability of model in the training set and validation set. (**C** and **D**) Time-dependent AUROC values in the training set and validation set. (**E–J**) Calibration curves for predicting 1-, 2-, and 3-year OS in the training set and validation set.

the RSF model had an AUC value above 0.7 for predicting any survival time point from 0 to 36 months in HBV-HCC patients (Figure 4C and D). They reflected good discrimination of the model. In addition, the calibration curves we plotted for the predictive model at 1-, 2-, and 3-year in both the training and validation sets fit the actual survival rates of HBV-HCC patients well, indicating that the RSF model had good calibration (Figure 4E–J). Our model also showed significant clinical benefits with DCA (Figure S1). Therefore, the RSF model performed satisfactorily. In addition, we compared the random survival forest model with other classical models used for prognostic assessment in HBV-HCC, such as the Child-Pugh score, ALBI score, and CLIP score. In both the training and validation cohorts, the random survival forest model demonstrated significantly superior predictive performance for 1-, 2-, and 3-year overall survival (OS) compared to the classical models (Table S4).

Application of RSF Model for Risk Stratification

Stratification of patients was important for guiding patient management. Patients with HBV-HCC were divided into high-risk group (with a risk score ≥ 17 points) and low-risk group (with a risk score < 17 points). The results of the Kaplan–Meier analysis and Log rank test between the high-risk group and low-risk group in the training and validation sets are presented in Figure 5A and B, which demonstrated a significant difference between the two groups (all $P < 0.0001$). Next, we showed that the risk group could function properly in different subgroups in patients with HBV-HCC. For instance, within the BCLC stage 0-B and C-D subgroups in the whole cohort, the low-risk subgroups exhibited substantially improved 3-year OS compared with the reference high-risk subgroups (Figure 5C and D). Similarly, the risk group could stratify patients with better or worse prognoses, both among patients with different AFP levels (Figure 5E and F). The clinical characteristics of the HBV-HCC
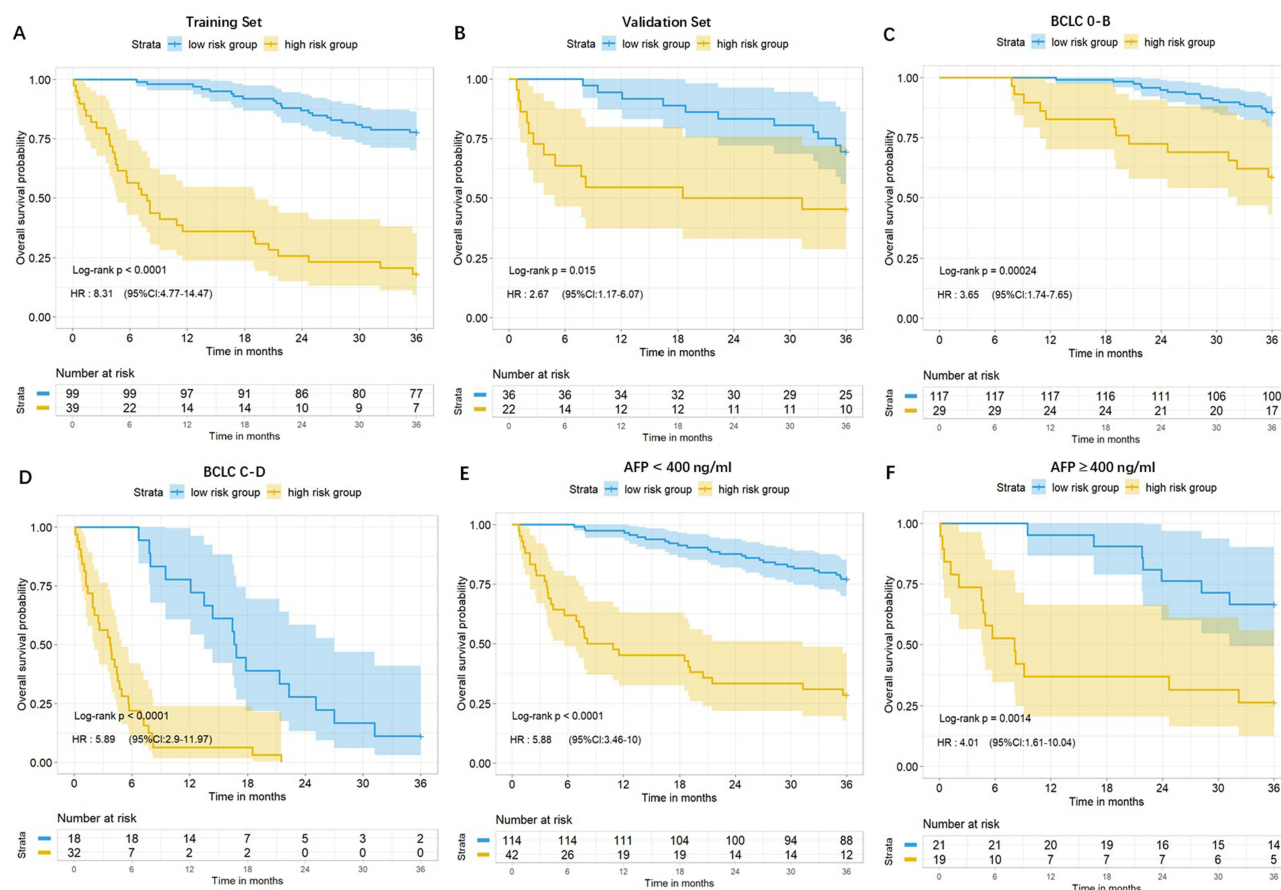

Figure 5 Risk stratification. (**A** and **B**) The patients were divided into low-risk and high-risk groups based on the risk score (low risk group < 17 points, high risk group ≥ 17 points) in the training set and validation set. (**C–F**) Kaplan-Meier analysis of 3-year OS in different BCLC staging and different levels of AFP in the whole cohort. The Log rank test was used to calculate the P value.

patients in the high- and low-risk groups were shown in Tables S5 and S6. As we can see, there were significant differences between the two groups in terms of BCLC staging, Child-Pugh stage, tumor size and immune status. Overall, these observations supported the robustness of the RSF model, as they indicated that the model could adapt to different event distributions and clinical staging systems.

Associations of sICs with Clinical Features and Membrane ICs

The Spearman correlation method was used to calculate the correlation coefficients for the parameters, including clinical characteristics, laboratory data, tumor-related indicators, and immunologic characteristics (Figure 6). As we can see, sPD-L1 was negatively correlated with hemoglobin (HGB) and positively correlated with AST and NLR ($P < 0.05$). Soluble TIM-3 level was negatively correlated with ALB and CD8+ T cells and positively correlated with HBV-DNA, AST, and LDH ($P<0.05$). In Figure 7A and B, the levels of sPD-L1 and sTIM-3 in HBV-HCC patients with BCLC stage C-D were higher than those in patients with BCLC stage 0-B (all $P < 0.05$). Patients with CD8+T cells < 320 cells/μL, AST ≥ 40 U/L, and CRP ≥ 5 mg/L had higher levels of sTIM-3 and sPD-L1 (all $P < 0.05$). The results indicated that higher levels of sPD-L1 and sTIM-3 were correlated with more severe immunosuppression, inflammation, and hepatocellular injury. Compared to the sPD-L1 and sGITR, sTIM-3 was correlated with more clinical indicators (Figure 6). Therefore, we aimed to evaluate the potential immune-regulatory role of sTIM-3 in the HBV-HCC and examined mTIM-3 by flow cytometry in CD4+ T cells, CD8+ T cells, and NK cells isolated from the peripheral blood of 80 hBV-HCC patients. As shown in Figure 7C, the level of sTIM-3 was positively correlated with mTIM-3 expression in CD8+ T cells ($P < 0.05$) and showed no correlation with mTIM-3 expression in CD4+ T cells and NK cells.
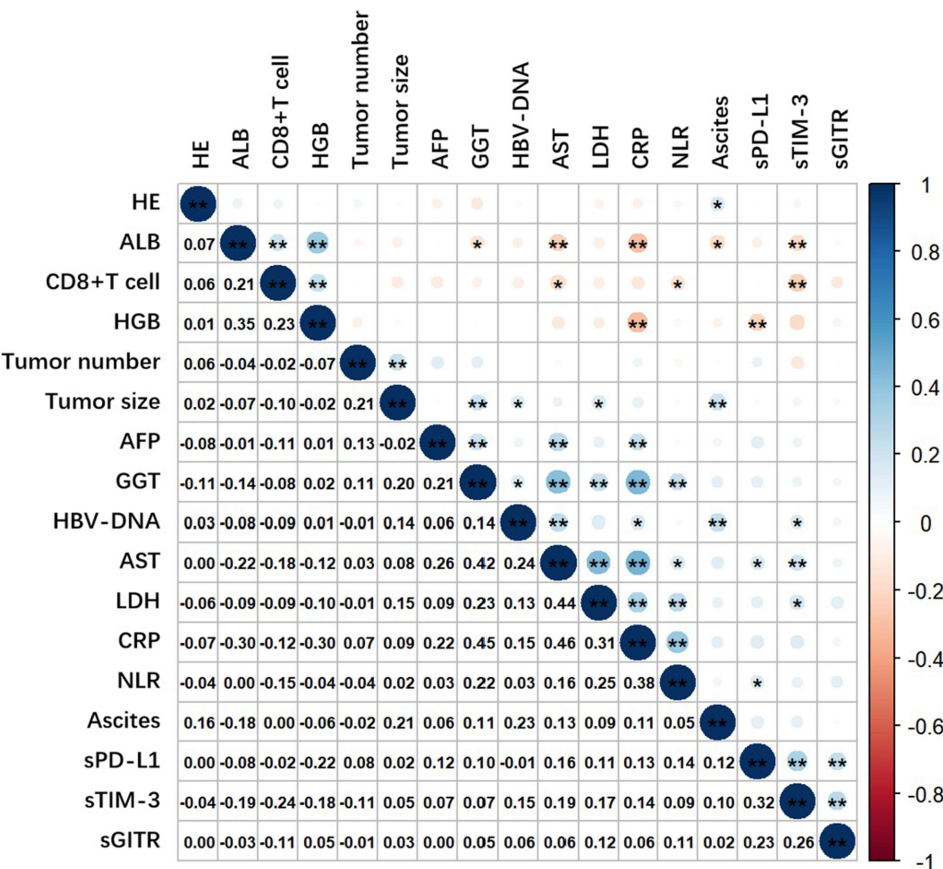
Figure 6 Correlation analysis. Heat map displaying the spearman's rank coefficient of correlations between three soluble immune checkpoints and clinical parameters. *p < 0.05; **p < 0.01; NS, no significance.
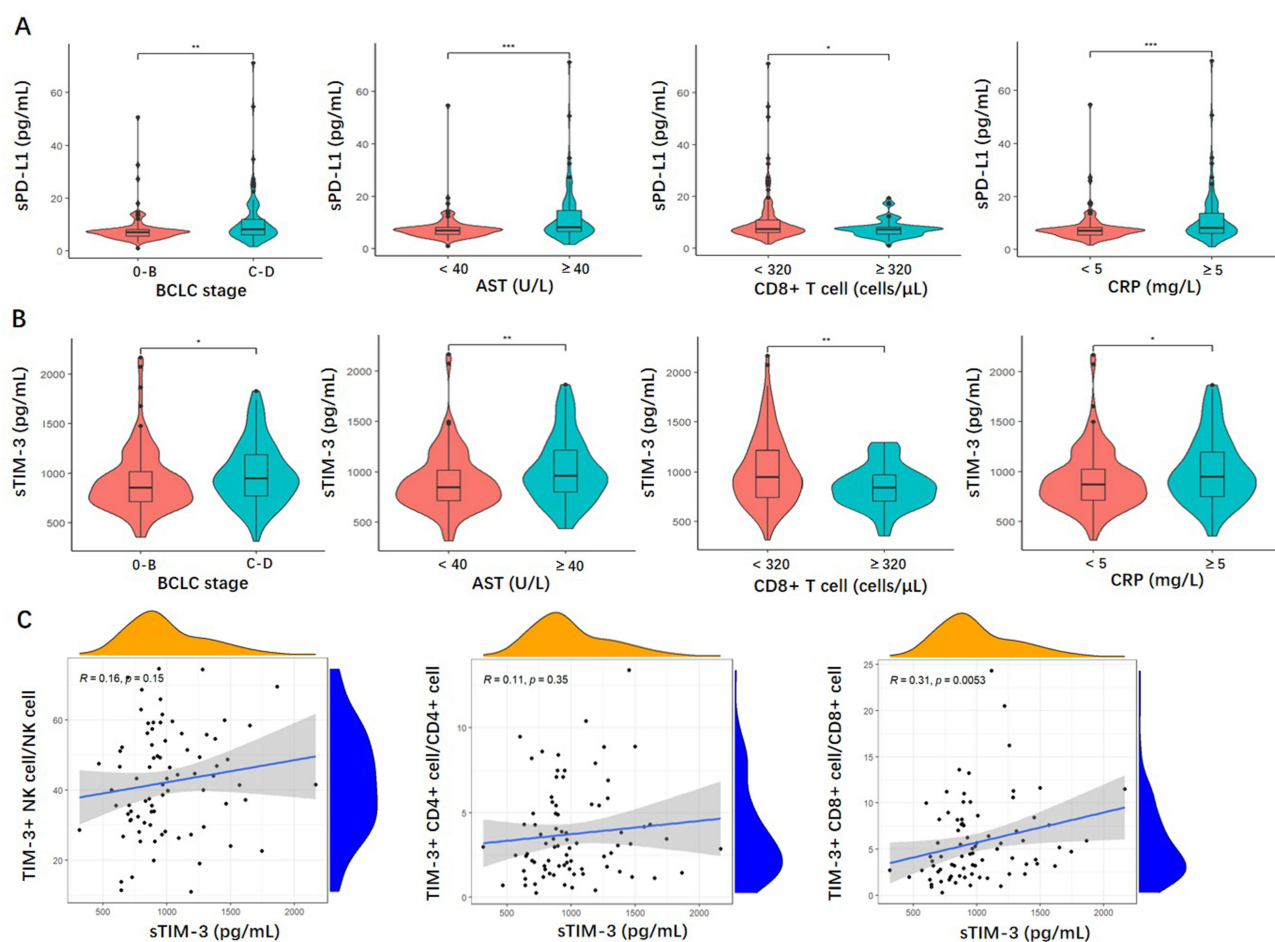
Figure 7 Associations of sICs with clinical features and membrane ICs. (**A** and **B**) Violin plots displaying differences of sPD-L1 and sTIM-3 levels in different BCLC stages and clinical parameters. (**C**) The correlation between membrane TIM-3 and sTIM-3. *p < 0.05; **p < 0.01; ***p < 0.001; NS, no significance.

Discussion

In this study, we systematically compared 14 sICs in four groups. The concentrations of 14 molecules were significantly higher in HBV-HCC groups than in healthy controls, suggesting a significant alteration in the immune status of HBV-HCC. Although there was a disease progression relationship between CHB, HBV-LC, and HBV-HCC, we did not observe a corresponding difference in the levels of sICs, which might be due to the small sample size.

We found that sGITR, sPD-L1 and sTIM-3 were negative risk factors for prognosis of HBV-HCC. These factors might be involved in the immune suppression of HBV-HCC. Researches have shown immune cell subsets in circulating blood and tumor micro-environment were immunosuppressed in HCC.[17] Our team's previous research has shown that compared to patients with chronic hepatitis B (CHB) or cirrhosis, the expression of programmed death protein 1 (PD-1) and T cell immunoreceptor with immunoglobulin and ITIM domain (TIGIT) in peripheral blood CD4+ T and CD8+T cells and the expression of T cell immunoglobulin and mucin domain 3 (TIM-3) and TIGIT in peripheral blood natural killer (NK) cells are significantly upregulated in HBV-HCC patients, which are associated with accelerated disease progression and poor outcomes in HBV-HCC.[18,19] In addition, the tumor microenvironment of HBV-HCC exhibits more severe immunosuppression and exhaustion than that of non-virus-associated HCC,[20] leading to a poor prognosis. Therefore, we suggest that immune indicators in cancer patients, such as sICs, should be monitored in the clinic.

Soluble immune checkpoints are important components of immune regulation, although their mechanisms of action have not yet been determined. Compared to immune markers in tumor tissues, sICs are easier to obtain, can be quantitatively detected, have low costs, and allow for rapid testing. They enable real-time monitoring of patients'

immune responses and disease progression, predict patient prognosis, evaluate treatment responses, and are less affected by tumor heterogeneity, which have significant potential in the era of liquid biopsy. The method for detecting sICs, Luminex, is an advanced multiplexing detection technology that integrates fluorescent encoded microspheres, laser analysis, flow cytometry, high-speed digital signal processing, and more scientific and technological achievements. It enables high-throughput, high-sensitivity parallel analysis of multiple indicators, improving detection efficiency and reducing costs. Its widespread use in cancer diagnosis and treatment would benefit patients with cancer.

Soluble TIM-3 was a negative prognostic factor for HBV-HCC. This molecule was produced by ADAM-10 and ADAM17-mediated cell membrane TIM-3 ectodomain shedding in human.[21,22] Some studies had shown that this protein was a negative immune-regulatory molecule. For instance, sTim-3 facilitated tumor growth in melanoma mice and inhibited T cell responses, as well as IL-2 and IFN-γ production in vitro. It significantly decreased anti-tumor CD8+ T cell activity and reduced the abundance of infiltrative lymphocytes in tumors.[13] The biological function of sTIM-3 might explain its negative prognostic value in HBV-HCC. Li et al reported that elevated sTIM-3 was associated with higher incidence and lower survival rate of HBV-HCC.[23] Chen et al found that sTIM-3 was a tumor prognostic factor and therapeutic target for the exhaustion of CD8+ T cell and anti-PD-1 resistance. Their team explored the underlying mechanisms: sTIM-3 induced the exhaustion of terminal T cells and weakened the response of CD8+ T cells to PD-1 inhibition by engaging with carcinoembryonic antigen-related cell adhesion molecule 1 (CEACAM-1). Additionally, the ADAM10 inhibitor GI254023X, which halted the generation of sTIM-3, slowed down tumor growth in mice with human-like Tim-3 and overcome resistance to PD-1 therapy in human tumor-infiltrating lymphocytes (TILs).[24] In addition, sTIM-3 might dimerize with mTIM-3 on T cells, enhancing inhibitory signaling through downstream targets like Bat3 phosphorylation, thus disrupting TCR signaling. This further validated our finding. Our study showed that sTIM-3 was positively correlated with mTIM-3 in CD8+ T cells which indicating that sTIM-3 might be a potential immunotherapy target for HBV-HCC. In addition, the levels of sTIM-3 were negatively correlated with ALB and CD8+ T cells and positively correlated with AST, LDH, CRP and HBV-DNA, suggesting that sTIM-3 was closely associated with abnormal liver function, inflammation, immunosuppression and HBV viral load.

GITR, initially described as a glucocorticoid-induced factor, was expressed on regulatory T (Treg) cells,[25] NK cells, and TILs.[26] It promoted the activation and proliferation of effector T cells and reduces Treg cells.[27] The cell sources of soluble GITR were macrophages and Tregs.[28] Studies have shown that sGITR triggers inflammatory processes in mice[11] and causes cell cycle arrest and apoptosis in murine macrophages[12] which result in a variety of immune responses. In our study, a high level of sGITR was closely associated with shorter survival in patients with HBV-HCC. Some studies reported that sGITR was a negative prognostic factor in patients with metastatic uveal melanoma and advanced solid tumors.[28,29] The reason might be that sGITR mediated immunosuppression by inhibiting the costimulatory molecule GITR/GITRL pathway, resulting in poor prognosis in patients with cancer. Further research is needed to focus on the mechanisms of this molecule. As for sPD-L1, our study showed that it was a negative prognostic factor in HBV-HCC. Study showed that sPD-L1 was associated with HBV infection and HBV-related liver disease progression.[7] Mechanistically, sPD-L1 combined with PD-1 to inhibit T-cell responses.[30] A study of systematic review and meta-analysis showed that sPD-L1 could be a good predictor for recurrence and survival after treatment for HCC.[31] In addition, sPD-L1 competed with mPD-L1 for PD-1 binding, inhibiting systemic T cells beyond the local TME. Therefore, sPD-L1 expression was associated with impaired immunity and poor prognosis. In addition, sPD-L1 levels were negatively correlated with HGB and CD8+ T cells, and positively correlated with AST, NLR, and CRP. This indicated that high sPD-L1 levels might reflect the severity of hepatocellular injury, persistent inflammation, and immunosuppression in patients with HBV-HCC.

The RSF model we constructed was based on tumor burden, liver function, inflammatory indicator and immune-related markers, which were clinically strongly associated with the prognosis of HCC. Factors incorporated into model included tumor size, sGITR, sPD-L1, hepatic encephalopathy, CD8+ cell, CRP, sTIM-3, AST, HBV-DNA and AFP. In recent years, an increasing number of studies have emerged that utilize artificial intelligence, including machine learning, to assist in clinical decision-making for HCC, achieving significant progress in risk prediction, diagnosis, and prognosis. In this study, we employed one of the machine learning algorithms, the RSF, to construct a predictive model. The RSF algorithm can handle and analyze a large number of variables without relying on the proportional hazards assumption, making it more flexible in dealing with survival data. By building multiple decision trees and summarizing their predictive results, it enhances the model's stability and robustness, reducing the risk of overfitting. The predictive performance of the RSF model we constructed is

acceptable, proving that the RSF can provide a novel model construction scheme. However, the use of a single modeling method may introduce assumption bias and result in poor generalizability. In the future, we look forward to RSF based on larger sample sizes and more convenient model visualization tools to assist in clinical decision-making for HCC.

Elevated baseline levels of sGITR, sPD-L1, and sTIM-3 might identify patients with T-cell exhaustion or an immunosuppressive microenvironment, who were less likely to respond to anti-PD-1/PD-L1 monotherapy. For instance, in HBV-HCC, high sPD-L1 might signal resistance to checkpoint inhibitors, suggesting combination therapies such as anti-PD-1 + anti-TIM-3 or VEGF inhibitors. Continuous monitoring of sICs during treatment can track immune reactivation or exhaustion. A post-treatment drop in sPD-L1 might indicate restored T-cell function, while a rise in sTIM-3 could imply adaptive immune evasion, necessitating early treatment adjustment. Moreover, dual blockade of membrane-bound and soluble checkpoints might be more effective for patients with high sGITR, sPD-L1, and sTIM-3 levels. The risk score was developed using RSF incorporated sIC levels into the decision-making framework to personalize immunotherapy regimens. We stratified the patients into risk groups based on this score, with those scoring less than 17 points classified as the low-risk group and those with 17 points or more as the high-risk group. Our risk stratification effectively distinguished patients with varying prognoses, aided in identifying potentially critical patients, enhanced disease prognosis assessment, and facilitated communication between healthcare providers and patients, as well as follow-up planning. For patients in the high-risk group, we were able to initiate treatment measures early on, reduce unnecessary examinations, and alleviate the strain on medical resources. Therefore, the model developed in this study could help predict survival in a clinical setting, which could help improve the outcomes in patients with HBV-HCC.

Our study had several limitations. First, excluding patients with severe organ diseases or incomplete data might introduce bias, affecting the validity and generalizability of the study results. If the excluded patients were more likely to have adverse outcomes or poorer treatment responses, the observed effect sizes might be overestimated. The findings might not be applicable to patients with comorbid organ diseases, limiting the clinical utility in a broader population. Secondly, the sensitivity and specificity of small validation sets might fluctuate significantly between different samples, increasing the uncertainty of the model's true generalization ability. In addition, it might not be able to detect overfitting and was more susceptible to sampling bias. Thirdly, single-center study typically reflected local demographic, clinical, or socioeconomic characteristics, limiting the applicability of the findings to broader or different populations. They might also be influenced by local healthcare policies, restricting their relevance to settings with fewer resources or different structures. It required multi-center, prospective external trials to verify our results. Lastly, the mechanism by which sICs affect the prognosis of HBV-HCC has not been elucidated in this section.

Conclusion

In conclusion, we developed a prognostic RSF model based on sICs for patients with HBV-HCC. sGITR, sPD-L1, and sTIM-3 were closely associated with the prognosis of patients with HBV-HCC. As potential therapeutic targets, these factors might synergize with existing immunotherapies to restore antitumor immunity. In addition, we acknowledged our study's limitations and the need for prospective clinical trials to validate our findings. Our next step is to investigate the correlation between the dynamic changes of sICs in the HBV-HCC cohort and immune therapy response. It is also important to standardize the sICs detection methods used in clinical practice to ensure cross-platform reproducibility. Future studies may apply these markers to test their predictive value for survival and potential immune functions in cancer.

Data Sharing Statement

The original contributions of the study are included in the article/supplementary material. Further inquiries can be directed to the corresponding author (Zhiyun Yang).

Ethics Approval and Consent to Participate

This study was conducted in accordance with the Declaration of Helsinki and approved by the Ethics Committee of Beijing Ditan Hospital, Capital Medical University (Beijing, China). At enrollment, written informed consent was obtained from all the participants, and corresponding blood samples and clinical data were collected.

Funding

Disclosure

The authors declare that they have no competing interests.

References

1. Sung H, Ferlay J, Siegel RL, et al. Global cancer statistics 2020: GLOBOCAN estimates of incidence and mortality Worldwide for 36 Cancers in 185 Countries. *CA Cancer J Clin*. 2021;71(3):209–249. doi:10.3322/caac.21660
2. Llovet JM, Kelley RK, Villanueva A, et al. Hepatocellular carcinoma. *Nat Rev Dis Primers*. 2021;7(1):6. doi:10.1038/s41572-020-00240-3
3. Toh MR, Wong EYT, Wong SH, et al. Global epidemiology and genetics of hepatocellular carcinoma. *Gastroenterology*. 2023;164(5):766–782. doi:10.1053/j.gastro.2023.01.033
4. Han CL, Tian BW, Yan LJ, et al. Efficacy and safety of immune checkpoint inhibitors for hepatocellular carcinoma patients with macrovascular invasion or extrahepatic spread: a systematic review and meta-analysis of 54 studies with 6187 hepatocellular carcinoma patients. *Cancer Immunol Immunother*. 2023;72(7):1957–1969. doi:10.1007/s00262-023-03390-x
5. Baudi I, Kawashima K, Isogawa M. HBV-Specific CD8+ T-Cell tolerance in the liver. *Front Immunol*. 2021;12:721975. doi:10.3389/fimmu.2021.721975
6. Han X, Gu YK, Li SL, et al. Pre-treatment serum levels of soluble programmed cell death-ligand 1 predict prognosis in patients with hepatitis B-related hepatocellular carcinoma. *J Cancer Res Clin Oncol*. 2019;145(2):303–312. doi:10.1007/s00432-018-2758-6
7. Xuan Hoan N, Minh Huyen P T, Dinh Tung B, et al. Association of PD-L1 gene polymorphisms and circulating sPD-L1 levels with HBV infection susceptibility and related liver disease progression. *Gene*. 2022;806:145935. doi:10.1016/j.gene.2021.145935
8. Zeng Z, Shi F, Zhou L, et al. Upregulation of circulating PD-L1/PD-1 is associated with poor post-cryoablation prognosis in patients with HBV-related hepatocellular carcinoma. *PLoS One*. 2011;6(9):e23621. doi:10.1371/journal.pone.0023621
9. Sagawa R, Sakata S, Gong B, et al. Soluble PD-L1 works as a decoy in lung cancer immunotherapy via alternative polyadenylation. *JCI Insight*. 2022;7(1). doi:10.1172/jci.insight.153323
10. Niu M, Liu Y, Yi M, Jiao D, Wu K. Biological characteristics and clinical significance of soluble PD-1/PD-L1 and Exosomal PD-L1 in Cancer. *Front Immunol*. 2022;13:827921. doi:10.3389/fimmu.2022.827921
11. Shin HH, Kim SG, Lee MH, Suh JH, Kwon BS, Choi HS. Soluble glucocorticoid-induced TNF receptor (sGITR) induces inflammation in mice. *Exp mol Med*. 2003;35(5):358–364. doi:10.1038/emm.2003.47
12. Shin HH, Kim SJ, Lee HS, Choi HS. The soluble glucocorticoid-induced tumor necrosis factor receptor causes cell cycle arrest and apoptosis in murine macrophages. *Biochem Biophys Res Commun*. 2004;316(1):24–32. doi:10.1016/j.bbrc.2004.02.012
13. Geng H, Zhang GM, Li D, et al. Soluble form of T cell Ig mucin 3 is an inhibitory molecule in T cell-mediated immune response. *J Immunol*. 2006;176(3):1411–1420. doi:10.4049/jimmunol.176.3.1411
14. Khan M, Zhao Z, Arooj S, Fu Y, Liao G. Soluble PD-1: predictive, prognostic, and therapeutic value for cancer immunotherapy. *Front Immunol*. 2020;11:587460. doi:10.3389/fimmu.2020.587460
15. Wang Q, He Y, Li W, et al. Soluble immune checkpoint-related proteins in blood are associated with invasion and progression in non-small cell lung cancer. *Front Immunol*. 2022;13:887916. doi:10.3389/fimmu.2022.887916
16. Khan M, Arooj S, Wang H. Soluble B7-CD28 family inhibitory immune checkpoint proteins and anti-cancer immunotherapy. *Front Immunol*. 2021;12. doi:10.3389/fimmu.2021.651634
17. Chew V, Lai L, Pan L, et al. Delineation of an immunosuppressive gradient in hepatocellular carcinoma using high-dimensional proteomic and transcriptomic analyses. *Proc Natl Acad Sci U S A*. 2017;114(29):E5900–e9. doi:10.1073/pnas.1706559114
18. Liu X, Li M, Wang X, et al. PD-1(+) TIGIT(+) CD8(+) T cells are associated with pathogenesis and progression of patients with hepatitis B virus-related hepatocellular carcinoma. *Cancer Immunol Immunother*. 2019;68(12):2041–2054. doi:10.1007/s00262-019-02426-5
19. Yu L, Liu X, Wang X, et al. TIGIT(+) TIM-3(+) NK cells are correlated with NK cell exhaustion and disease progression in patients with hepatitis B virus-related hepatocellular carcinoma. *Oncoimmunology*. 2021;10(1):1942673. doi:10.1080/2162402x.2021.1942673
20. Lim CJ, Lee YH, Pan L, et al. Multidimensional analyses reveal distinct immune microenvironment in hepatitis B virus-related hepatocellular carcinoma. *Gut*. 2019;68(5):916–927. doi:10.1136/gutjnl-2018-316510
21. Möller-Hackbarth K, Dewitz C, Schweigert O, et al. A disintegrin and metalloprotease (ADAM) 10 and ADAM17 are major sheddases of T cell immunoglobulin and mucin domain 3 (Tim-3). *J Biol Chem*. 2013;288(48):34529–34544. doi:10.1074/jbc.M113.488478
22. Clayton KL, Douglas-Vail MB, Nur-ur Rahman AK, et al. Soluble T cell immunoglobulin mucin domain 3 is shed from CD8+ T cells by the sheddase ADAM10, is increased in plasma during untreated HIV infection, and correlates with HIV disease progression. *J Virol*. 2015;89 (7):3723–3736. doi:10.1128/jvi.00006-15

23. Li F, Li N, Sang J, et al. Highly elevated soluble Tim-3 levels correlate with increased hepatocellular carcinoma risk and poor survival of hepatocellular carcinoma patients in chronic hepatitis B virus infection. *Cancer Manag Res*. 2018;10:941–951. doi:10.2147/cmar.S162478

24. Chen C, Zhao F, Peng J, et al. Soluble Tim-3 serves as a tumor prognostic marker and therapeutic target for CD8(+) T cell exhaustion and anti-PD-1 resistance. *Cell Rep Med*. 2024;5(8):101686. doi:10.1016/j.xcrm.2024.101686

25. Sakaguchi S, Sakaguchi N, Asano M, Itoh M, Toda M. Immunologic self-tolerance maintained by activated T cells expressing IL-2 receptor alpha-chains (CD25). Breakdown of a single mechanism of self-tolerance causes various autoimmune diseases. *J Immunol*. 1995;155 (3):1151–1164. doi:10.4049/jimmunol.155.3.1151

26. Vence L, Bucktrout SL, Fernandez Curbelo I, et al. Characterization and comparison of GITR expression in solid tumors. *Clin Cancer Res*. 2019;25 (21):6501–6510. doi:10.1158/1078-0432.Ccr-19-0289

27. Kraehenbuehl L, Weng CH, Eghbali S, Wolchok JD, Merghoub T. Enhancing immunotherapy in cancer by targeting emerging immunomodulatory pathways. *Nat Rev Clin Oncol*. 2022;19(1):37–50. doi:10.1038/s41571-021-00552-7

28. Botticelli A, Pomati G, Cirillo A, et al. The role of immune profile in predicting outcomes in cancer patients treated with immunotherapy. *Front Immunol*. 2022;13:974087. doi:10.3389/fimmu.2022.974087

29. Rossi E, Zizzari IG, Di Filippo A, et al. Circulating immune profile can predict survival of metastatic uveal melanoma patients: results of an exploratory study. *Hum Vaccin Immunother*. 2022;18(3):2034377. doi:10.1080/21645515.2022.2034377

30. Liang Z, Chen W, Guo Y, et al. Soluble monomeric human programmed cell death-ligand 1 inhibits the functions of activated T cells. *Front Immunol*. 2023;14:1133883. doi:10.3389/fimmu.2023.1133883

31. Xue JS, Liu H, Meng GX, et al. Prognostic value of soluble programmed cell death-1 (sPD-1) and soluble programmed cell death ligand-1 (sPD-L1) for hepatocellular carcinoma: a systematic review and meta-analysis. *Cancer Immunol Immunother*. 2022;71(7):1633–1644. doi:10.1007/ s00262-021-03103-2